

Vibrational effects on the reaction of NO_2^+ with C_2H_2 : Effects of bending and bending angular momentum

Jason M. Boyle, Brady W. Uselman, Jianbo Liu,^{a)} and Scott L. Anderson^{b)}

Department of Chemistry, University of Utah, 315 S. 1400 E. Rm. 2020, Salt Lake City, Utah 84112, USA

(Received 27 December 2007; accepted 8 February 2008; published online 18 March 2008)

NO_2^+ in six different vibrational states was reacted with C_2H_2 over the center-of-mass energy range from 0.03 to 3.3 eV. The reaction, forming $\text{NO}^+ + \text{C}_2\text{H}_2\text{O}$ and $\text{NO} + \text{C}_2\text{H}_2\text{O}^+$, shows a bimodal dependence on collision energy (E_{col}). At low E_{col} , the reaction is quite inefficient (<2%) despite this being a barrierless, exoergic reaction, and is strongly inhibited by E_{col} . For $E_{\text{col}} > \sim 0.5$ eV, a second mechanism turns on, with an efficiency reaching $\sim 27\%$ for $E_{\text{col}} > 3$ eV. The two reaction channels have nearly identical dependence on E_{col} and NO_2^+ vibrational state, and identical recoil dynamics, leading to the conclusion that they represent a single reaction path throughout most of the collision. All modes of NO_2^+ vibrational excitation enhance both channels at all E_{col} , however, the effects of bend (010) and bend overtone (02⁰⁰) excitation are particularly strong (factor of 4). In contrast, the asymmetric stretch (001), which intuition suggests should be coupled to the reaction coordinate, leads to only a factor of ~ 2 enhancement, as does the symmetric stretch (100). Perhaps the most surprising effect is that of the bending angular momentum, which strongly suppresses reaction, even though both the energy and angular momentum involved are tiny compared to the collision energy and angular momentum. The results are interpreted in light of *ab initio* and Rice-Ramsperger-Kassel-Marcus calculations. © 2008 American Institute of Physics.

[DOI: 10.1063/1.2889953]

I. INTRODUCTION

In studying complex reaction mechanisms, it is useful to have a variety of probes that each are sensitive primarily to different steps in the mechanism. In our approach to this problem, we use the effects of reactant vibrational excitation as a probe of the early time dynamics, based on the idea that the initial mode of excitation is scrambled by any strong perturbations, such as the formation or breaking of bonds.¹ Therefore, if significant mode-specific effects are seen, this implies that the rate-limiting step in the mechanism is early, and provides insight regarding which kinds of molecular motions are important. Product recoil velocity distributions probe reaction time scales and disposition of the available energy into the products, i.e., the middle and late stages of the mechanism. When measured over a range of collision energies (E_{col}), and combined with theory, the mechanism can be unraveled in detail.^{2,3}

While there is now a significant body of work probing effects of vibrational excitation mode on different classes of reactions, there is little information about the effects of vibrational angular momentum associated with bending of linear molecules. A number of studies of effects on energy transfer in low energy collisions have been reported,⁴ however, we are aware of only two previous studies looking at effects on reactions. One, from our group,² studied energy transfer in NO_2^+ -rare gas collisions leading to dissociation, and found a small but reproducible difference in dissociation

cross section for the bend overtone state with and without bending angular momentum. The other, from Kreher *et al.*⁵ compared (among other states) the effect of exciting the (11¹⁵) and (105) overtone combination band of HCN on the reaction with Cl to yield HCl+CN. Little difference was observed between the reactivity of the two states, even though both the bend quantum number and angular momentum changed. Here we report a very large (factor of ~ 2) effect of simply changing from the (02⁰⁰) state to the (02²⁰) state, even though both the energy difference (2 meV) and bend angular momentum are negligible compared to the energy and angular momentum of the collisions.

II. EXPERIMENTAL AND COMPUTATIONAL DETAILS

A. Experimental details

NO_2^+ is produced by two color, three photon ionization, resonant at the two photon level with the $E^2\Sigma_u^+(3p\sigma)$ Rydberg state, as described previously.⁶ State purity is measured by photoelectron spectroscopy to be better than 96% for all states probed in this study. The ionization scheme allows the production of NO_2^+ in its ground state, with one quantum in any of the three vibrational modes or with two quanta of bending excitation. The fundamental levels, labels, and energies are as follows: Symmetric stretch (1,0,0) with 170 meV, asymmetric stretch (0,0,1) with 290 meV, and bend with (0,1,0) 78 meV. We can also produce ions in two levels associated with the overtone of the bend. The (0,2⁰,0) level (153 meV) corresponds to planar bending motion. The (0,2²,0) level (155 meV) corresponds classically to NO_2^+

^{a)}Also at Department of Chemistry and Biochemistry, Queens College of CUNY, 65-30 Kissena Blvd., Flushing, NY 11367.

^{b)}Electronic mail: anderson@chem.utah.edu.

having one quantum of bending each in the xz and yz planes, 90° out of phase, resulting in a molecule with fixed bend angle, rotating at the vibrational frequency.

The differential cross section measurements were made in a guided-ion beam scattering instrument described in detail previously,^{7,8} along with our calibration and data analysis procedures. Briefly, a 1:5 mixture of NO_2 in He was passed through a pulsed valve, and the resulting molecular beam was collimated by a skimmer before entering the ionization region. Ionization occurred just inside the end of a radio frequency (rf) quadrupole ion guide that focused the ions into a quadrupole mass filter, which, for this system, was also operated as an ion guide (rf only). The time-of-flight (TOF) gating at the end of this second quadrupole was used to narrow the temporal and kinetic energy distributions of the NO_2^+ reactant beam and to reject NO^+ fragment ions produced in the resonantly enhanced multiphoton ionization source. The state- and kinetic-energy-selected ions were injected into an eight-pole rf ion guide, that guided them through a scattering cell filled with acetylene to 2×10^{-4} Torr. This pressure was chosen to provide reasonable signal for the small reaction cross sections in this system, while keeping multiple collision effects to an insignificant level. Unreacted NO_2^+ ions, together with any product ions, were collected by the ion guide, and passed into a second ion guide for TOF velocity analysis. Finally, the ions were mass analyzed and counted using a multichannel scalar. Integral cross sections were calculated from the ratio of product and reactant ion intensities, using the calibrated effective length of the scattering cell.⁷ The width of the ion kinetic energy distribution (~ 0.15 eV) and zero of the center-of-mass collision energy (E_{col}) scale was measured by TOF. TOF was also used to measure the axial velocity (v_{axial}) distributions for the NO^+ and $\text{C}_2\text{H}_2\text{O}^+$ products, i.e., the projection of the full two-dimensional distributions on the ion guide axis.

The $\text{NO}_2^+ + \text{C}_2\text{H}_2$ reaction is quite inefficient, thus many data sets (cross sections versus vibrational state and collision energy) were required to achieve a reasonable signal-to-noise ratio. Because the measurements are time-consuming, a typical day's data do not include cross sections for all NO_2^+ vibrational states, however, each data set includes a measurement for ground state NO_2^+ . In averaging data sets taken over a period of a month, we used the ground state cross section as an indicator of possible instrumental problems, such as potential barriers in the ion guides that block the transmission of low energy ions. If the ground state cross section for a particular day deviated by more than 10% from the average of all the data sets, then *all* data from that day were discarded. The data presented are averages of the retained data sets, and error bars are taken from the standard deviations. The relative error in comparing cross sections for different states is estimated to be 15%, which includes both random error and our best estimate of possible sources of systematic error (e.g., day to day variations in ion beam energy distribution shape). In addition, we estimate about a 20% uncertainty in the absolute scale of the cross sections, due to factors such as uncertainty in the scattering cell pressure-length product and possible mass-dependence of the final mass spectrometer transmission efficiency.

B. Computational details

To construct a reaction coordinate and to get energetic information, *ab initio* structure optimizations were performed at the B3LYP/6-311++G** level of theory, using GAUSSIAN 03.⁹ For all stable structures found, the calculations were repeated at the MP2/6-311++G** and G3 levels of theory. The energetic trends for the three levels of theory were consistent. The B3LYP/6-311++G** level of theory was chosen because it best agrees with single point calculations done at the QCISD(T)/cc-pVTZ level of theory. Geometries were optimized calculating the force constants at every point. The resulting vibrational frequencies and zero-point energies were scaled by factors of 0.9613 and 0.9804, respectively.⁹ All transition states (TSs) were verified to be first order saddle points by frequency calculations, and intrinsic reaction coordinate (IRC) calculations were used to determine which potential wells are connected by all the TS structures that were found.

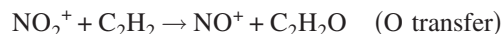
After standard TS-searching algorithms failed repeatedly to find a key transition state (TS2) for the breakup of one of the intermediate complexes, we performed trajectory calculations to identify better starting geometries for TS searching. Trajectories were started at the equilibrium geometry of the complex, with randomly distributed internal energy equivalent to what the complex would have in a 1 eV collision. TS searches were then started from a number of likely looking high potential energy geometries, leading to identification of TS2, which was shown to be the desired TS by IRC calculations.

To examine the kinetic consequences of the various complexes and TSs, Rice-Ramsperger-Kassel-Marcus (RRKM) rate and density-of-state calculations were performed with the program of Zhu and Hase,¹⁰ using its direct state count algorithm, and energetics, moments of inertia, and vibrational frequencies (scaled) from the B3LYP/6-311++G** calculation.

III. RESULTS

A. Integral cross sections

Product ions are observed at masses 30 and 42 corresponding to O and O^+ transfer reactions,



$$\Delta H_{\text{rxn}} = -2.98 \text{ eV.}$$



where the energetics are experimental,¹¹ and refer to the most stable structure of the $\text{C}_2\text{H}_2\text{O}^{(+)}$ product in each case (see below). Note that the two channels differ only in which product carries the charge, i.e., they are simply the lowest two electronic states of $[\text{NO} + \text{C}_2\text{H}_2\text{O}]^+$. The integral cross sections for O and O^+ transfer in reaction of ground state NO_2^+ with C_2H_2 are shown in Fig. 1, over the center-of-mass collision energy (E_{col}) range from 0.03 to 3.5 eV. Also shown in the inset are the total reaction cross section (σ_{total}) and an estimate of the collision cross section ($\sigma_{\text{collision}}$), taken as the greater of the capture cross section (σ_{capture}) and the hard

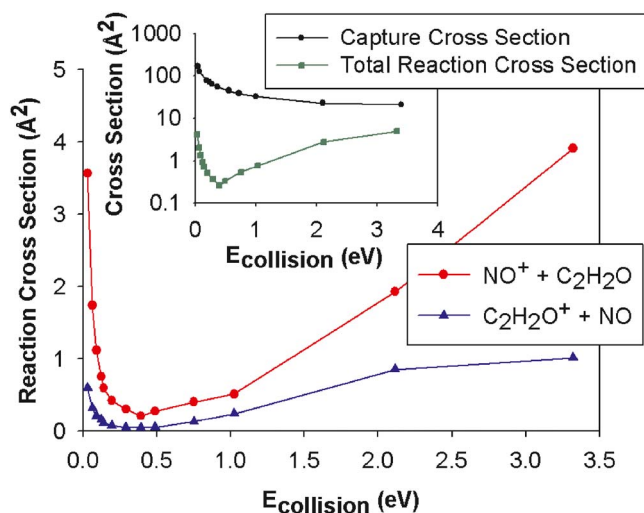


FIG. 1. (Color online) Ground state reaction cross section vs collision energy. Inset: total cross section and the estimated collision cross section.

sphere cross section ($\sigma_{\text{hard sphere}}$). $\sigma_{\text{hard sphere}}$ was calculated from the orientation-averaged contact radii of NO_2^+ and C_2H_2 , assuming covalent radii for each atom, and exceeds σ_{capture} for $E_{\text{col}} > 2.5$ eV.

The two channels have similar dependence on E_{col} , although O transfer dominates over the entire range of E_{col} , with O/O⁺ transfer branching ratios ranging from ~ 6 at low E_{col} , dropping to ~ 2 for E_{col} around 1 eV, then returning to ~ 4 for high E_{col} . The fact that the cross sections rise sharply with decreasing E_{col} at low E_{col} shows that both channels are barrierless (i.e., there are no barriers on the reaction coordinate in excess of the reactant energy). Nonetheless, the reaction efficiency, i.e., $\sigma_{\text{total}}/\sigma_{\text{collision}}$, is only $\sim 2\%$ at our lowest energy point (~ 0.03 eV). Reactivity falls sharply with increasing energy, such that for E_{col} near 0.4 eV, the reaction efficiency is only $\sim 0.5\%$. At higher energies, both channels are enhanced by collision energy, such that the reaction efficiency reaches 27% at our highest energy point. This pattern suggests the presence of a severe bottleneck to reaction, and that collision energy inhibits the passage of the bottleneck for $E_{\text{col}} < 0.4$ eV, but allows the system to bypass the bottleneck at higher E_{col} .

B. Computational results

The *ab initio* results for the $\text{NO}_2^+ + \text{C}_2\text{H}_2$ system are summarized in Fig. 2 and Table I. One important point is that there are two isomers of both $\text{C}_2\text{H}_2\text{O}$ and $\text{C}_2\text{H}_2\text{O}^+$, giving rise to four possible product channels. For both $\text{C}_2\text{H}_2\text{O}$ and $\text{C}_2\text{H}_2\text{O}^+$, the ketene (H_2CCO) isomer is substantially more stable than the ethynol (HCCOH) isomer, although all four channels are exoergic. The energetics used in Fig. 2 are experimental¹¹ for reactants and for the ketene isomer of the product channels. Energetics for complexes, transition states, and the ethynol product isomer ($[\text{NO} + \text{HCCOH}]^+$) are from B3LYP/6-311++G** calculations.

Four complexes that might mediate reaction were found. There is an electrostatically bound reactantlike complex (RC) ~ 0.5 eV below the reactant energy. In this complex, the charge is partly delocalized, such that the Mulliken

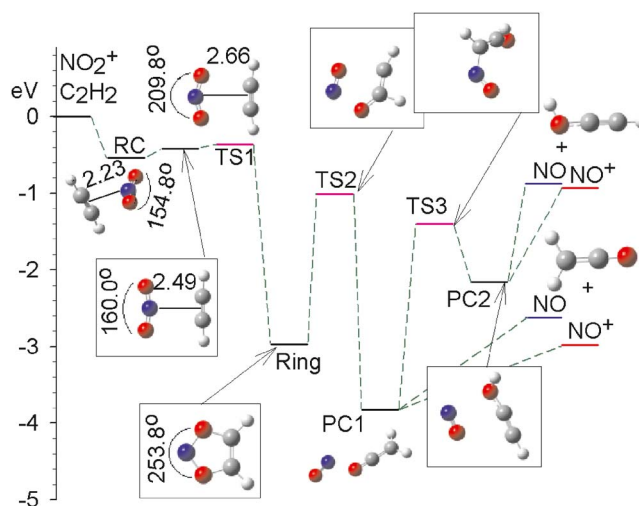


FIG. 2. (Color online) Reaction coordinate for $\text{NO}_2^+ + \text{C}_2\text{H}_2$.

charges are 0.66 and 0.34 for the NO_2 and C_2H_2 moieties, respectively. The partial charge transfer in RC is reflected by an ONO bond angle (155°) that is intermediate between the values calculated for NO_2^+ (linear) and NO_2 (134°) at this level of theory. Because this complex can form from reactants with no rearrangements, no barrier to its formation is expected.

Complexes PC1 and PC2 are analogous electrostatically bound complexes of the ketene and ethynol isomeric products, respectively, each bound by ~ 1 eV with respect to the corresponding product asymptotes. In PC1, the Mulliken charge is nearly equally shared between the NO and H_2CCO moieties while in PC2 the NO moiety carries $\sim 65\%$ of the charge. Because the dissociation energies of PC1 and PC2 to products are small compared to the available energy (> 0 eV for all E_{col}), their lifetimes will be short, and they are unlikely to be dynamically significant. In addition, such productlike complexes clearly come after the rate-limiting step on the reaction coordinate, and therefore cannot influence the measured vibrational or collision energy effects on reactivity. The high energy and tightness of TS3, compared to the orbiting TSs governing dissociation of PC1 to $[\text{NO} + \text{H}_2\text{CCO}]^+$ products, implies that both kinetic and energetic factors should strongly favor the ketene isomeric products. Therefore, the ethynol ($[\text{NO} + \text{HCCOH}]^+$) product channels are expected to be negligible at all collision energies.

In addition to these weakly bound electrostatic complexes, there is a covalently bound, five-membered ring complex (“ring”) with C_{2v} symmetry and a binding energy of ~ 3 eV with respect to reactants. We were unable to locate any stable covalently bound complexes where only a single CO bond is formed (see below). The ring complex can be accessed from RC by rotating the reactants into a C_{2v} geometry, then passing over TS1, which lies only 0.18 eV above RC. The imaginary vibrational frequency corresponding to the reaction coordinate at TS1 is ~ 70 cm^{-1} . The calculation of the IRC connecting the ring to PC1 via TS2 indicates that as the ring falls apart, first one C–O bond breaks, then the N–O bond breaks at TS2, which then rearranges by a

TABLE I. Experimental and *ab initio* energies (eV) relative to reactants ($\text{NO}_2^+ + \text{C}_2\text{H}_2$).

	B3LYP/6-311++G** ^a	MP2/6-311++G**	G3 (0 K)	Experimental ^b
$\text{NO}^+ + \text{CH}_2\text{CO}$	-2.54	-2.35	-2.58	-2.98
$\text{NO} + \text{CH}_2\text{CO}^+$	-2.68	-1.60	-2.30	-2.62
$\text{NO}^+ + \text{HCCOH}$	-0.93		-1.09	-1.66
$\text{NO} + \text{HCCOH}^+$	-0.88		-0.38	
Reactant complex	-0.54		-0.44	
Ring complex	-2.97		-2.90	
Product complex 1	-3.74			
Product complex 2	-2.16			
TS1	-0.36			
TS2	-1.01			
TS3	-1.40			

^aIncluding the zero-point energy calculated at B3LYP/6-311++G** and scaled by 0.9804.

^bNIST Chemistry Web Book (Ref. 19).

1,2-hydrogen shift, yielding PC1. PC1 can then form the ketene product channels, with no barrier in excess of the dissociation energy. The minimum energy reaction path outlined here (reactants \rightarrow RC \rightarrow TS1 \rightarrow ring \rightarrow TS2 \rightarrow PC1 \rightarrow products) is consistent with the experimental finding that the reaction is barrierless. To account for the very low reactivity and unusual E_{col} dependence, we need to consider the kinetics expected for such a reaction path, as discussed below.

C. Recoil velocity distributions

TOF data were collected for product ions at a series of collision energies and for each vibrational state. Laboratory frame axial velocity (v_{axial}) distributions for the NO^+ product of the O transfer channel are given in the top four frames of Fig. 3, for E_{col} ranging from 0.41 to 3.35 eV. Because the cross section for $\text{C}_2\text{H}_2\text{O}^+$ production (O^+ transfer) is so small, only the v_{axial} distribution for $E_{\text{col}} = 3.35$ eV is shown (bottom frame). The points are the raw v_{axial} data, and the smooth curves are fits based on simulations of the experiments (*vide infra*). The solid vertical lines in each frame indicate the laboratory velocity of the center-of-mass frame, averaged over the collision energy distribution ($\langle V_{\text{c.m.}} \rangle$). The dashed vertical lines indicate the product ion velocities predicted by the spectator-stripping mechanism V_{SS} .¹² Axial velocity (v_{axial}) distributions are simply projections of the full velocity distributions on the ion guide axis. Because our experiment is axially symmetric, the laboratory frame v_{axial} distributions can be approximately converted to the center-of-mass (c.m.) frame simply by subtracting $\langle V_{\text{c.m.}} \rangle$. The raw laboratory-frame v_{axial} distributions, thus, provide useful dynamical insight. For example, if reaction is mediated by a complex with lifetime ($\tau_{\text{collision}}$) greater than its rotational period (τ_{rotation}), the resulting v_{axial} distribution must be symmetric about $\langle V_{\text{c.m.}} \rangle$. Conversely, an asymmetric v_{axial} distribution is a clear sign that reaction is direct (i.e., not complex-mediated), and also reveals the dominant scattering mechanism (i.e., forward versus backward scattering). Finally, some insight into the partitioning of available energy into product recoil can be inferred from displacement of the v_{axial} distribution with respect to $\langle V_{\text{c.m.}} \rangle$.

There are a few limitations of this technique, as implemented here. Product ions that are strongly backscattered in the c.m. frame may have negative laboratory frame velocities. To collect such ions, the lens at the ion guide entrance is biased positive relative to the guide potential, reflecting these ions toward the detector. The reflected ions arrive at long flight times, appearing as if they had low, but positive laboratory velocities. In addition, the slowest ions are most likely to have their velocities perturbed by small inhomogeneities in the surface potentials on the ion guides or by secondary collisions. Finally, these distortions in the low velocity portion of the v_{axial} distributions are exacerbated by the singular TOF-to-velocity Jacobian. For these reasons, v_{axial} data below 500 m/s are given zero weight in the fitting process used to extract information from the distributions. Here, the problem is serious only for low E_{col} (because $V_{\text{c.m.}}$ is small), therefore we show and analyze data only for $E_{\text{col}} > 0.4$ eV.

For ground state reactant ions at high E_{col} , the velocity distribution for NO^+ from the O-transfer channel is asymmetric (Fig. 3, second frame from bottom), peaking well forward of (i.e., faster than) $V_{\text{c.m.}}$, but with a substantial tail extending into the backward (slower than $V_{\text{c.m.}}$) direction. The bottom frame shows that the corresponding distribution for the O^+ transfer channel is also asymmetric, but backward peaked relative to $V_{\text{c.m.}}$. Note, however, that we define “forward” and “backward” as product *ions* with laboratory velocity greater or smaller, respectively, than $V_{\text{c.m.}}$. Therefore, in comparing a pair of channels such as $\text{NO}^+ + \text{C}_2\text{H}_2\text{O}$ and $\text{C}_2\text{H}_2\text{O}^+ + \text{NO}$, the dynamical sense of forward/backward is reversed. In this case, the velocity peak for both channels corresponds to small angle scattering, i.e., to a mechanism wherein NO_2^+ transfers O or O^+ to the C_2H_2 reactant, with the NO^+ or NO product continuing along in the same general direction as the original velocity of NO_2^+ reactant. As E_{col} is reduced, the distributions become increasingly symmetric, and by 0.4 eV, the distribution is forward-backward symmetric within experimental error. Because of the small cross section for O^+ transfer, and kinematics that are less favorable for resolving structure in the $\text{C}_2\text{H}_2\text{O}^+$ v_{axial} distribution, it is not possible to say if the same transition to symmetric distributions occurs for the $\text{C}_2\text{H}_2\text{O}^+$ product.

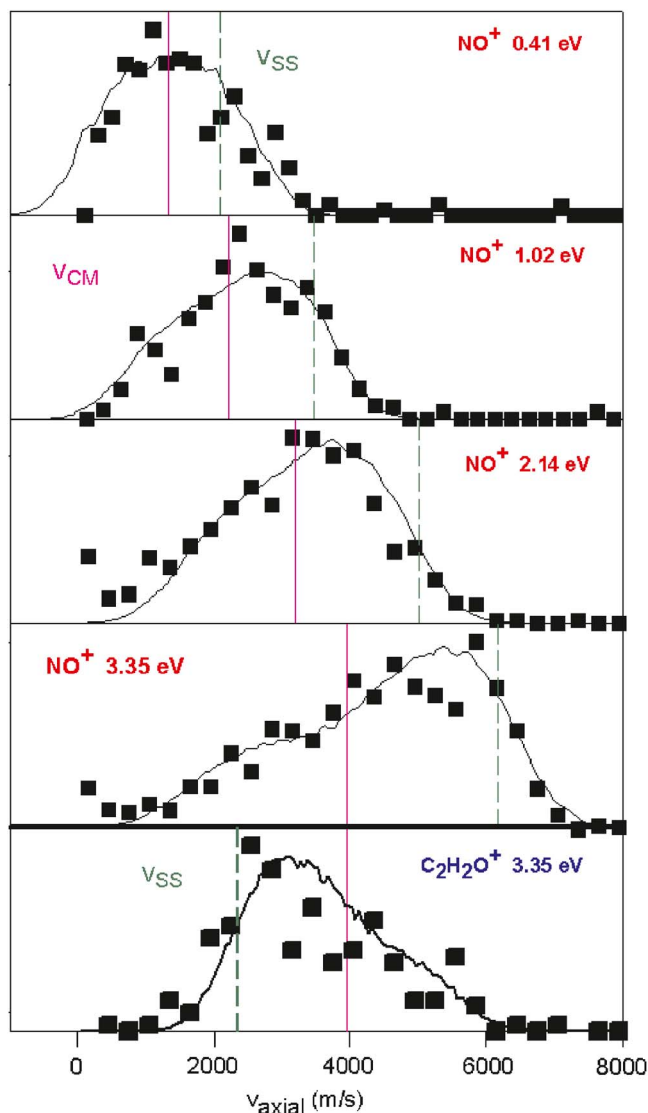


FIG. 3. (Color online) Axial recoil velocity distributions for the NO^+ channel (top four frames) and $\text{C}_2\text{H}_2\text{O}^+$ channel (bottom frame). Points are experimental. Solid curves are simulations. Solid vertical line is $\langle V_{\text{c.m.}} \rangle$. Dashed vertical line is $\langle V_{\text{SS}} \rangle$.

To extract a more quantitative picture, it is necessary to fit the data, thereby correcting for the broadening that results from the distributions of NO_2^+ and C_2H_2 reactant velocities. Our fitting program and procedures have been described previously.⁷ In essence, a model recoil velocity distribution is assumed, and then run through a Monte Carlo simulation of the experiment to include the effects of all broadening factors. The resulting convoluted v_{axial} distribution is compared with experiment, and the input parameters of the

model are varied to optimize the fit. Because the data are only projections of the full velocity distribution, it is important to use a model that is physically reasonable, but which depends on only a few parameters. Here, both the v_{axial} and RRKM results suggest that the mechanism may involve a short-lived complex at low E_{col} , transitioning to direct scattering with increasing energy.

The osculating complex model¹³ was developed to describe angular distributions in just such systems, and has been used here for that purpose. In the model, a fleeting complex is assumed to form, with lifetime τ_{complex} and rotational period τ_{rotation} . It is also assumed that in absence of any complex rotation, the products would scatter at some particular angle θ_{peak} , here assumed to be either 0° or 180° , depending on whether the measured distribution is forward or backward peaked. The rotation of the complex broadens the angular distribution, and the extent of measured forward-backward asymmetry determines the ratio $\tau_{\text{collision}}/\tau_{\text{rotation}}$. Because τ_{rotation} can be estimated from the moment of inertia of the complex and the available angular momentum, the forward-backward asymmetry is directly related to the complex lifetime. Assuming a complexlike RC in Fig. 2, τ_{rotation} drops smoothly from ~ 0.9 ps at $E_{\text{col}}=0.1$ eV to ~ 0.4 ps at $E_{\text{col}}=3.0$ eV. The other input needed to simulate the recoil velocity measurements is a model for the recoil energy distribution $P(E_{\text{recoil}})$. Here, $P(E_{\text{recoil}})$ is assumed to be a Gaussian parametrized in terms of the energy available to the products (E_{avail}). The parameter describing the peak fraction of E_{avail} going into recoil (f_{peak}) is constrained by the measured displacement of the v_{axial} peak from $V_{\text{c.m.}}$. The fractional width parameter (f_{width}) is constrained by the shape of the high (or low) v_{axial} fall-off. In summary, the model is physically reasonable, all four parameters are dynamically significant, and each is constrained by a different feature of the measured v_{axial} distributions.

The fits are shown as solid curves in Fig. 3, and the corresponding fit parameters are summarized in Table II. It is important to note that the fit shown for the $\text{C}_2\text{H}_2\text{O}^+$ channel at 3.35 eV was done using the same parameter values that gave the best fit to the NO^+ channel at the same E_{col} , with the exception that θ_{peak} was taken as 180° , rather than 0° . In both cases, the parameters correspond to short collision times, 19% of E_{avail} in recoil, and a propensity for small angle scattering. Clearly the O and O^+ transfer channels have very similar recoil dynamics, at least for high E_{col} .

D. Vibrational effects

All modes of NO_2^+ vibrational excitation enhance both O and O^+ transfer reactions at all collision energies, albeit

TABLE II. Fit results for $\text{NO}^+ v_{\text{axial}}$ distributions.

E_{col} (eV)	$\langle E_{\text{avail}} \rangle^{\text{a}}$ (eV)	$\langle E_{\text{recoil}} \rangle$ (eV)	$\langle E_{\text{recoil}} \rangle / \langle E_{\text{avail}} \rangle$ (%)	$\tau_{\text{collision}}$ (ps)	$\tau_{\text{fly-by}}^{\text{b}}$ (ps)
0.411	2.98	0.36	12	1.3	0.23
1.07	3.64	0.47	12	0.21	0.14
2.19	4.76	0.57	12	0.17	0.10
3.33	5.90	1.10	19	0.10	0.08

^a $\langle \rangle$ = mean value.

^b $\tau_{\text{fly-by}}$ defined as time for reactants to travel a relative distance of 0.5 \AA .

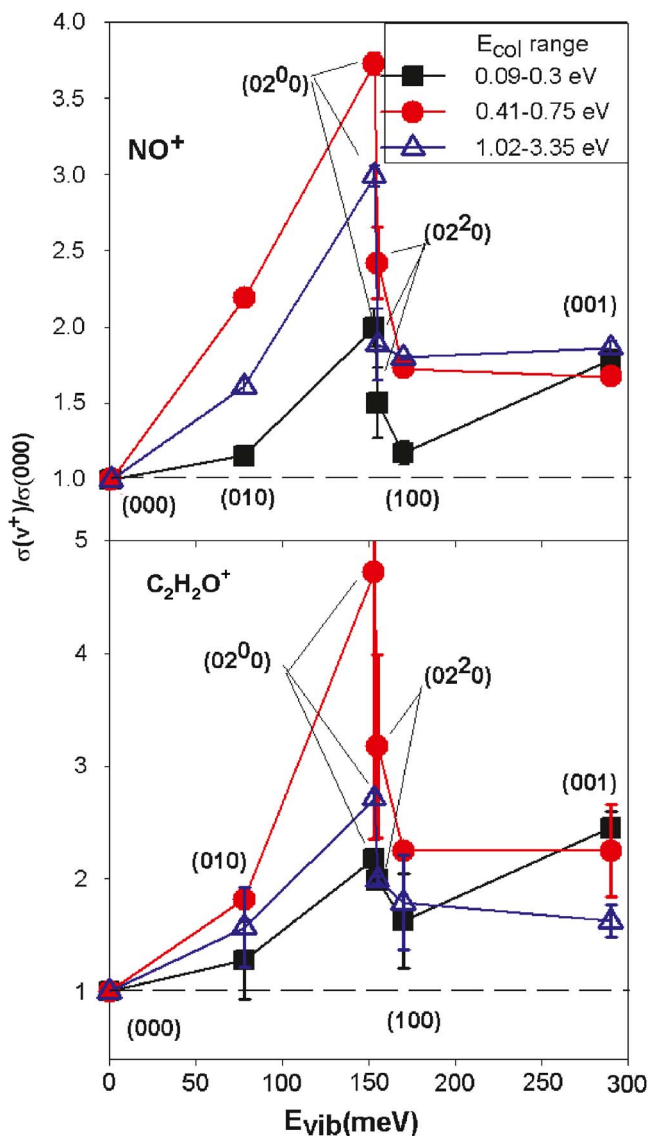


FIG. 4. (Color online) Vibrational enhancement factors vs vibrational energy, and averaging collision energy points within the indicated ranges.

with strong dependence on vibrational mode. To better show the vibrational effects, Fig. 4 gives vibrational enhancement factors for each NO_2^+ reactant state plotted against the vibrational energy E_{vib} . Each point corresponds to a particular NO_2^+ reactant state, indicated by the labels. The enhancement factors are simply ratios of the cross section for reaction of a particular state $\sigma(\nu^+)$ to the cross section for reaction for the ground state $\sigma(\text{gs})$. Results are shown for three E_{col} ranges of interest, and to reduce the uncertainties in the ratios the data for E_{col} points within each range were averaged. Error bars are the standard deviations. Where not shown, they are smaller than the height of the symbols.

Note that both the magnitudes and mode dependence of the vibrational effects are nearly identical for O and O^+ transfer, again suggesting that the channels are dynamically linked. Because the larger O-transfer cross sections lead to smaller uncertainties, we will focus the discussion on that channel. Note that while all modes enhance both reactions, the relative effects (*per unit* E_{vib}) of NO_2^+ bending excitations ((0,1,0) and (0,2,0)) are much greater than those of the

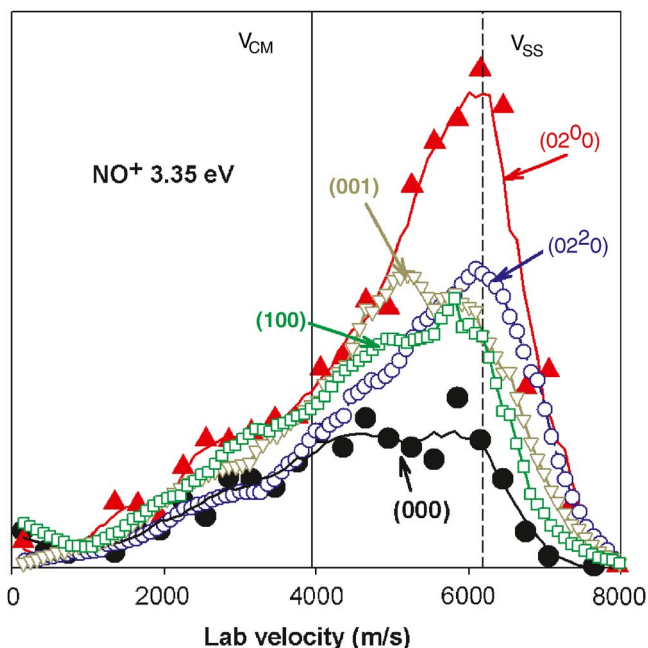


FIG. 5. (Color online) Axial recoil velocity distributions for the (000), (100), (001), (02⁰0), and (02²0) states at 3.35 eV collision energy. Solid vertical line: $\langle V_{\text{cm}} \rangle$. Dashed vertical line: $\langle V_{\text{SS}} \rangle$.

symmetric (1,0,0) and asymmetric stretch (0,0,1) modes. There is also a substantial difference in the effects from excitation of the (0,2⁰,0) and (0,2²,0) states, even though they differ by only ~ 3 meV.

Figure 5 shows the effects of NO_2^+ vibrational excitation on the NO^+ v_{axial} distributions for $E_{\text{col}}=3.35$ eV. Vibrational effects on the distributions for other collision energies above 1 eV are similar, although the distributions gradually become less forward peaked, as shown in Fig. 3. A detailed comparison at energies below 1 eV was not attempted because the v_{axial} distributions are relatively featureless (Fig. 3). The data for each vibrational state are scaled such that the integral under each curve is proportional to the measured integral cross section for that state. For the (000) and (02⁰0) states, the raw data are shown as large filled symbols, along with curves obtained by smoothing the data. For the other states, where the distributions overlap and are hard to follow because of noise in the raw data, we show only the smoothed data, plotted with small, open symbols to allow the three curves to be distinguished. Excitation of all four excited states preferentially enhances the forward-scattered component of the v_{axial} distribution, such that the ratio of forward-scattered to backward-scattered intensity increases from ~ 1.8 for the ground state to ~ 3.5 for the (02⁰0) state, with the other states lying in between.

In addition, it can be seen that different reactant modes have different effects on the shape of the distributions. For example, excitation of either bend overtone [(02⁰0) or (02²0)] shifts the corresponding v_{axial} distribution to higher velocities such that it peaks at the spectator stripping velocity V_{SS} . The two stretch excitations (100) or (001) give enhancement factors similar to that for (02²0) excitation, however, the v_{axial} distributions continue to peak well below V_{SS} , similar to that for the ground state.

IV. DISCUSSION

The $\text{NO}_2^+ + \text{C}_2\text{H}_2$ reaction was previously studied, both experimentally and computationally, by Bernardi *et al.*¹⁴ The experiments included Fourier transform-ion cyclotron resonance measurements using charge transfer with Xe^+ to produce NO_2^+ ions with $E_{\text{internal}} < \sim 2.5$ eV. It is likely that much of this excitation was in the bend mode, owing to the bent-to-linear geometry change when NO_2 is ionized. For some experiments, the NO_2^+ was collisionally relaxed prior to reaction. They did not report rate constants or branching ratios, but stated that both NO^+ and $\text{C}_2\text{H}_2\text{O}^+$ product channels were observed for internally hot NO_2^+ , but that only NO^+ was seen if the NO_2^+ was relaxed. Based on our results, which extend down to the thermal kinetic energy range, we suspect that they simply did not have the sensitivity to see the minor $\text{C}_2\text{H}_2\text{O}^+$ channel for ground state reactants. Given the enhancements we observe for modest levels of NO_2^+ vibrational excitation, it is likely that their reaction rates for hot NO_2^+ were large enough for both channels to be detected.

Bernardi *et al.* found three reaction pathways at the MP2/6-311+G* level linking the reactants to the observed product masses, all of which correlated to the ketene product isomer. In our study at the B3LYP/6-311++G** level, we only found the pathway (also found by them) through the five-membered ring complex shown in Fig. 2. The other pathways involve intermediates such as four-membered rings that we found to be unstable or well above the reactant energy at the B3LYP/6-311++G** level. From their Metastable Ion Kinetic Energy Spectroscopy study of decomposition of $\text{C}_2\text{H}_2\text{NO}_2^+$, they concluded that the five-membered ring pathway is the only one significant in this reaction, and as shown below, this single pathway is sufficient to account for our measurements as well. Further discussion of the effects of theoretical method on the computed reaction coordinate(s) will be given when we in a report a study (in progress) exploring this system with trajectory methods.

A. Product channel coupling and branching

One aspect of the reaction mechanism for this system that appears to hold across the entire E_{col} range probed, is that the O and O^+ transfer channels are strongly coupled. The two channels have similar E_{col} dependence (Fig. 1), vibrational effects (Fig. 4), and product scattering dynamics (Fig. 3). Mode-specific effects probe early time dynamics, before collisional interactions have scrambled the initial mode of excitation. The recoil dynamics probe both collision time scale (forward-backward asymmetry) and energy partitioning into the products [$P(E_{\text{recoil}})$]. The similarities between the channels indicate that the channels are coupled throughout most of the collision process, and such a picture is consistent with the reaction coordinate shown in Fig. 2. In essence, the reaction takes place on a single potential surface up to PCI, with charge delocalized as long as the inter-reactant or inter-product separation is small. It is only when the products finally separate that the charge has to localize on either the NO or $\text{C}_2\text{H}_2\text{O}$ moieties, and because localization is so late in the collision, the two channels show nearly identical dynam-

ics. In this scenario, we might expect that the branching between $\text{NO}^+ + \text{C}_2\text{H}_2\text{O}$ and $\text{C}_2\text{H}_2\text{O}^+ + \text{NO}$ channels should be controlled largely by the relative energetics in the two channels, which favor NO^+ production by 350 meV. Experimentally, the $\text{NO}^+/\text{C}_2\text{H}_2\text{O}^+$ branching ratio falls with increasing E_{col} from ~ 6 at our lowest E_{col} to ~ 2 for E_{col} between 1 and 2 eV, then increases again to ~ 4 at $E_{\text{col}} = 3.2$ eV.

If branching is controlled by product channel energetics, then statistically the branching would simply reflect the ratio of the densities of states (DOSs ratio) for the two channels. The DOS ratio will clearly fall with increasing E_{col} as the energy difference between the channels (350 meV) becomes small compared to E_{avail} . Note, however, that even at our lowest E_{col} , 350 meV is less than 12% of E_{avail} , thus the experimental branching ratio (~ 6) seems surprisingly large. To estimate the DOS ratio more quantitatively, we calculated the DOS for the $\text{NO}^+ + \text{C}_2\text{H}_2\text{O}$ and $\text{NO} + \text{C}_2\text{H}_2\text{O}^+$ channels, using the experimental energetics, scaled vibrational frequencies from the *ab initio* results, orbiting TSs for both channels, and the direct state count algorithm in the RRKM program of Zhu and Hase.¹⁵ The resulting ratio falls smoothly from ~ 2.5 at our lowest E_{col} to ~ 1.8 at $E_{\text{col}} = 3$ eV. In other words, the DOS ratio is about a factor of 2 smaller than the experimental branching ratio at low E_{col} , and less strongly dependent on E_{col} —both factors consistent with the fact that the channel energy difference is small compared to the exoergicity. We conclude that statistical factors probably account for some of the measured propensity toward the $\text{NO}^+ + \text{C}_2\text{H}_2\text{O}$ channel in the $E_{\text{col}} \leq 2$ eV range, but that other factors are probably also at work.

The observed doubling of the branching ratio as E_{col} increases from 2 to 3.3 eV is clearly opposite to the trend expected from a statistical perspective. A possible contributing factor is collision-induced dissociation (CID) ($\text{NO}_2^+ + \text{C}_2\text{H}_2 \rightarrow \text{NO}^+ + \text{O} + \text{C}_2\text{H}_2$), contributing only to the NO^+ branching. CID has a threshold of 2.85 eV for the spin-forbidden channel producing $\text{O}(^3P)$, whereas the spin-allowed channel is inaccessible in our study [E_0 for $\text{O}(^1D)$ production = 4.82 eV]. We recently studied CID of NO_2^+ in collisions with rare gases,² and found that the spin-forbidden channel is reasonably efficient for Xe, presumably due to the strong spin-orbit coupling in this fourth row atom; however, for Kr and the lighter rare gases, only the spin-allowed channel is observed. In fact, for Ne and Ar, the CID cross section is insignificant for E_{col} below ~ 8 eV, thus it seems unlikely that CID contributes significantly to the NO^+ signal or branching ratio for the energy range here.

A factor that may well influence product branching is vibrational dynamics in the exit channel. For example, the NO^+ bond length¹⁶ is ~ 0.09 Å shorter than that of NO, thus the relative energetics of the two channels will vary depending on how the NO moiety is distorted as the product separation distance reaches the critical range where the charge must localize. Similar arguments apply to distortions of the H_2CCO moiety. Vibrational dynamics this late in a rearrangement reaction are expected to essentially be unaffected by the reactant vibrational state, consistent with the negligible effects observed of the reactant state on product branching ratio. On the other hand, it is not unreasonable to

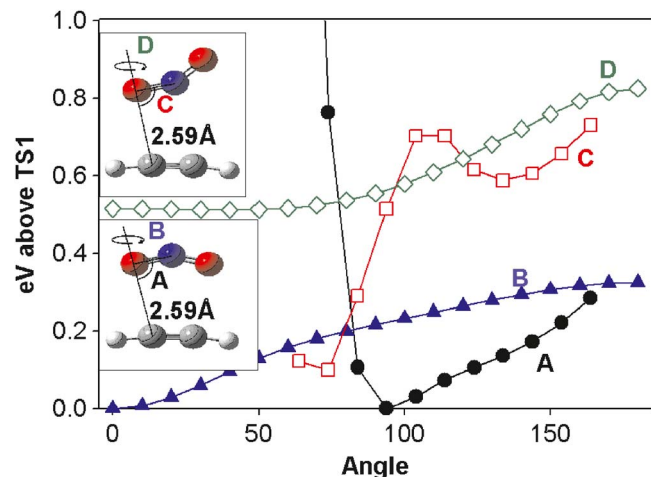


FIG. 6. (Color online) Cuts through the potential energy surface near TS1 for the indicated distortions of the TS1 structure. Energies are relative to TS1.

expect that as the products separate from a high energy, constrained geometry such as TS2, the potential surface may impart particular vibrational motions that might significantly influence branching, and because the product separation dynamics and timescale will change with E_{col} these effects may vary nonmonotonically.

Regardless of what factors control branching, it is clear that the O and O⁺ transfer channels are coupled well past the rate-limiting point on the reaction coordinate. Therefore, in the balance of this discussion, we will treat them as a single channel. For most purposes we will focus on the NO⁺+C₂H₂O data, because the larger signal allows more detailed analysis.

B. Reaction mechanism at low collision energies

It is apparent in Fig. 1, that reactions at low and at high E_{col} occur by different mechanisms, and that neither mechanism is efficient at energies between about 0.3 and 0.5 eV. We focus first on the low E_{col} mechanism.

The fact that the low E_{col} reaction efficiency rises sharply with decreasing E_{col} , but remains quite inefficient (~2%), implies a bottleneck to reaction, the passage through which is strongly inhibited by E_{col} . TS1, with its need to make two simultaneous CO bonds, is a plausible candidate for such a bottleneck. We tested this hypothesis by exploring the potential energy surface near TS1, using single point calculations at the B3LYP/6-311++G** level to map how the energetics change as the structure is distorted in various ways. Note that TS1 is only ~0.4 eV below reactants, thus small changes in energy are sufficient to block passage for low E_{col} . The results are given in Fig. 6, where the energies are all referenced to TS1. In essence, any distortion that prevents simultaneous formation of both nascent CO bonds raises the energy significantly, particularly if one CO distance is shortened significantly (curve A) while the other remains at the long distance found in TS1 (2.60 Å). Note also that it is important for the NO₂ moiety to bend such that the N atom is away from the C₂H₂. In any geometries where the N atom is bent toward C₂H₂, even at long

inter-reactant separation, the energy is substantially higher. The exception is if angle C is reduced enough to allow C–N bond formation, the energy drops, however, this is a mechanistic dead end, i.e., does not lead to products. We conclude that the strong dependence of energy on geometry around TS1 is sufficient to account for the low reactivity.

The increase in reaction efficiency at high energies is clearly consistent with Fig. 6—given enough energy the system can react in a wide range of geometries. The sharp increase in efficiency at very low energies requires a different enhancement mechanism. A plausible scenario is that a complex mediates reaction at low energies, providing time for the reactants to find their way through TS1 along the minimum energy path. The forward-backward symmetric v_{axial} distributions at low E_{col} are necessary, but there is no sufficient evidence supporting complex mediation at energies up to ~0.5 eV. The question is whether any of the complexes on the reaction coordinate are stable enough to support a mechanistically significant complex.

RRKM calculations were performed for all the complexes shown in Fig. 2, using vibrational energies and rotational constants from the B3LYP/6-311++G** calculations. For decay of RC to reactants and of PC1 and PC2 to products, we assumed orbiting transition states, and otherwise used TS1–TS3 as appropriate. To estimate the angular momentum in the complexes, we assumed complex formation governed by capture, i.e., used the impact parameter-weighted average angular momentum for capture collisions at each energy. As suggested above, the productlike complexes PC1 and PC2 are mechanistically insignificant, i.e., decay is 100% to the corresponding products, and the RRKM lifetimes are negligible. Figure 7 gives the RRKM results for both the RC and ring complex. We give the complex lifetimes and the forward-branching ratio, i.e., the fraction of complex decay that tends to carry the system toward products, as opposed to back to reactants. Also shown are the rotational period of the complex and the “fly-by” time, given as a measure of how long a “direct” collision would last at the same collision energy. The fly-by time was arbitrarily taken as the time for reactants to move 5 Å relative to each other—surely an upper limit on the time during which strong inter-reactant forces would be active in a direct encounter.

The ring complex is stabilized by relatively large barriers at TS1 and TS2, resulting in a lifetime longer than the rotational period for E_{col} up to ~1 eV. This complex, therefore, could account for the forward-backward symmetric v_{axial} distributions observed at low E_{col} . Note, however, that the forward branching ratio for the ring complex is near unity over this energy range, i.e., if a statistical ring complex forms at low collision energies, it almost always goes on to products. In that case, the rate-limiting step has to come before the ring complex, therefore this complex cannot affect reactivity, including the low E_{col} reactivity spike and vibrational effects.

The RC is weakly bound, and has a mechanistically significant lifetime ($\tau_{\text{complex}} > \tau_{\text{fly-by}}$) only for E_{col} below 0.1 eV. Furthermore, the forward-branching ratio falls off quickly with energy, such that RC decay would contribute little to the net product signal above 0.1 eV. Experimentally, the low E_{col}

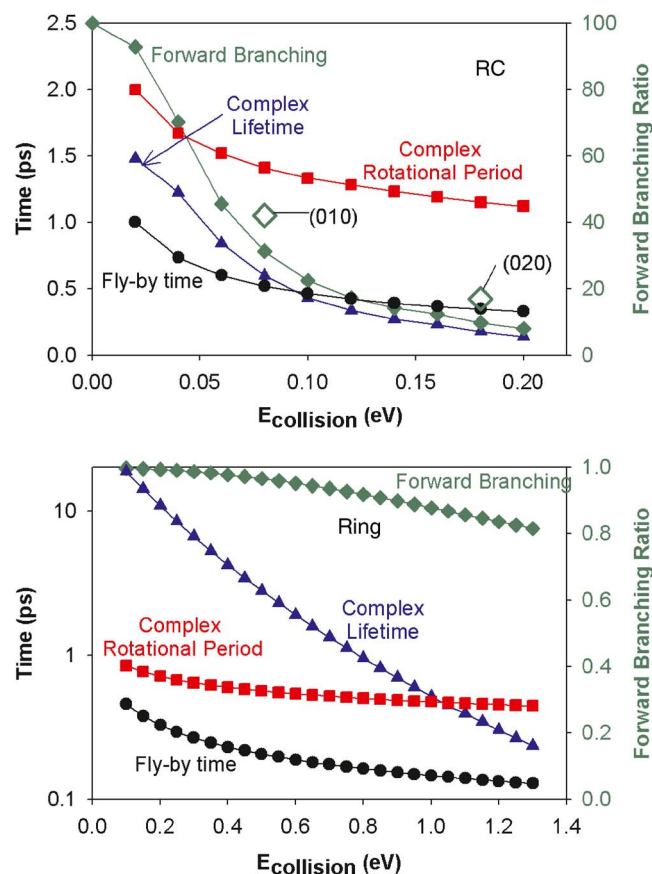


FIG. 7. (Color online) Left hand scales: RRKM lifetime and rotational period vs collision energy for the RC (top) and ring (bottom) complexes, compared to fly-by time (see text). Right hand scale: forward branching ratios.

reactivity spike is somewhat broader than 0.1 eV, however, we note that there is a ~ 170 meV collision energy distribution at low E_{col} , implying that the actual reactivity spike is quite sharp. We conclude, therefore, that mediation by this weakly bound reactantlike complex is sufficient to account for the low E_{col} mechanistic component. Furthermore, comparing the forward branching ratios for RC and ring complexes, it is clear that the rate-limiting point, at least in a statistical mechanism, is TS1, i.e., formation of the ring complex. Finally, while RC enhances reaction probability at $E_{\text{col}} < 0.1$ eV, it cannot account for symmetric v_{axial} distributions up to ~ 0.5 eV. It seems, therefore, that both complexes are important at low E_{col} , with RC controlling reactivity, and the ring complex stretching the collision time sufficiently to account for the forward-backward symmetry.

The properties of RC and TS1 appear sufficient to account for the strong inhibition by E_{col} at low energies within a statistical mechanism. On the other hand, the vibrational effects observed at our lowest energies are inconsistent with a purely statistical mechanism. In such a mechanism, E_{col} and E_{vib} are not expected to be equivalent, because adding E_{col} also increases the available angular momentum. The angular momentum tends to suppress reaction, because the orbiting TS governing decay back to reactants is substantially looser than TS1, thus we might expect that E_{vib} should cause less inhibition than the equivalent amount of E_{col} . To illus-

trate this effect, Fig. 7 also shows the effect on forward branching of adding vibrational energy equivalent to one or two quanta of the bend (large open diamonds). For this calculation, RC was given energy and angular momentum corresponding to the lowest E_{col} point plus the appropriate E_{vib} . Note that the RRKM model predicts less inhibition from E_{vib} than from E_{col} , but strong inhibition nonetheless. In contrast, the experiments show strong and mode-specific vibrational enhancement at low energies. Vibrational effects are discussed further below.

C. Reaction at high energies

A new mechanism clearly turns on for $E_{\text{col}} > \sim 0.4$ eV eventually reaching 27% efficiency at high E_{col} . This energy is well past the range where complexes can have any significant effect on the scattering, thus the limiting mechanism must be direct. The v_{axial} distributions support this scenario—as the E_{col} is increased, the distributions become increasingly asymmetric. Note, however, that even at $E_{\text{col}} = 3.35$ eV, where the collision energy dependence has flattened out, the v_{axial} distributions are far from the stripping limit, with a substantial backward-scattered component. Within the osculating complex model, this backward component is attributed to collisions where the complex rotated $\sim 180^\circ$ before decaying to products. Clearly, in the high energy limit, the complex lifetimes are too short to allow significant rotation (Fig. 7), therefore, we need to reinterpret the v_{axial} distributions. In the limit of negligible complex rotation, the forward-scattered component corresponds to large impact parameter collisions, wherein NO_2^+ transfers O, and the nascent NO^+ continues forward. (The same is true for the backward-scattered component of the O^+ transfer channel.) This mechanism is essentially stripping, but there is clearly considerably more translational-to-internal energy conversion than in the spectator stripping limit. If the impact parameter is the primary determinant of scattering angle, then the backward-scattered NO^+ (or forward-scattered $\text{C}_2\text{H}_2\text{O}^+$) corresponds to collisions at small impact parameters, leading to product rebound. Of course at intermediate energies, the v_{axial} distributions presumably depend on both impact parameter and the effects of (ring) complex rotation.

One question is what sets the limiting high energy reaction efficiency at 27%. At low energies, the O/ O^+ transfer reaction path requires a very constrained geometry (TS1) so that two CO bonds can form simultaneously. At high energies, the relatively high reaction efficiency implies that a considerably wider range of reactant geometries is reactive, consistent with the potential surface cuts in Fig. 6. If we assume that O/ O^+ transfer can occur in geometries with only one strongly interacting C–O pair, then 27% efficiency seems reasonable. Note, however, that the strong vibrational enhancements, particularly from the bend, imply that reactivity is controlled by more than just the impact geometry, even at high E_{col} .

D. Vibrational effects

This system shows strong and quite mode-specific enhancements from NO_2^+ vibrational excitation (Fig. 4). Bend-

ing is particularly efficient, with effects approximately linear in bending energy for the (010) and (02⁰⁰) states, however, the bend overtone enhancement is roughly halved, if the state with angular momentum (02²⁰) is selected. Finally, the two stretches give even smaller enhancements, despite these being the highest energy modes. One point to note is that the (100) mode is in Fermi resonance with the (02⁰⁰) mode. Grant¹⁷ has shown that the mixing from the Fermi resonance is at the $\sim 10\%$ level, i.e., the mode we label (100) has $\sim 90\%$ symmetric stretch character and $\sim 10\%$ bend overtone character. Conversely, the mode we label (02⁰⁰) is $\sim 90\%$ bend overtone and $\sim 10\%$ symmetric stretch. Presumably, if it were possible to prepare the unmixed bend overtone and symmetric stretch states, the already large difference in vibrational effect would be somewhat larger.

As discussed above, the low E_{col} reactivity spike is attributed to trapping into the complex RC, thereby increasing collision time and the chance that the system can find the low energy pathway through TS1. It is conceivable, albeit unlikely, that addition of NO_2^+ vibrational excitation somehow enhances trapping into RC, and thereby enhances the complex-mediated mechanism. As shown in Fig. 7, however, the suppressing effect of E_{vib} on forward branching (and lifetime) is so large as to cancel any hypothetical enhancement of complex formation. Instead, we propose that NO_2^+ vibration has its effect at TS1, even though TS1 comes after RC on the reaction coordinate. It is interesting to compare the period of the different vibrations with the collision time scale. The classical vibrational periods associated with the fundamentals of the different modes range from 54 fs for the bend (010) to ~ 14 fs for the asymmetric stretch (001). The collision time scale is somewhat arbitrary, however, at low E_{col} the relevant scale is the RC lifetime (Fig. 7). (The ring complex is irrelevant here because it comes after the rate-limiting point on the reaction coordinate, and thus can have no effect on reactivity.) Over the E_{col} range of the reactivity spike, the RC lifetime is at least an order of magnitude longer than any of the vibrational periods. The proposed mechanism, therefore, implies that the initial NO_2^+ vibrational state must remain largely uncoupled to other modes of RC for $>$ ten periods, so that it can influence the breakup of the complex, increasing the branching through TS1 to products. If reactant vibration did couple in RC, the additional energy in the active modes of the complex would strongly inhibit reaction as shown in Fig. 7.

Presumably the observed pattern of mode effects indicates that particular molecular motions help drive the system toward the TS1 geometry, and thus shift the RC decay branching toward products. The large bending enhancement is reasonable because the NO_2 moiety in TS1 is strongly bent. This scenario also accounts for the relatively weak effects of the symmetric and asymmetric stretches, because TS1 is symmetric with NO bond lengths similar to those in NO_2^+ . The additional energy in either stretch mode would strongly inhibit reaction if randomized in the complex; therefore the observed weak enhancements imply that the stretch modes also remain mostly uncoupled in RC, and exert some control over the decay branching, possibly by weakening the geometric constraint to passing through TS1.

The idea that reactant vibrational excitation can survive in many vibrational periods in a weakly bound reactantlike complex, then influence the branching during complex decay, is an important result of mode-selective studies. Such behavior has been observed in other systems with weakly bound reactantlike complexes, including some with considerably stronger, and longer-lived complexes than RC (e.g., $\text{C}_6\text{H}_5\text{OH}^+ + \text{ND}_3$, with $E_{\text{binding}} \sim 1.2$ eV and RRKM $\tau_{\text{complex}} \sim 1$ ns).¹⁸

At high E_{col} , both reaction efficiency and strippinglike dynamics indicate that reaction can occur in asymmetric geometries where only one NO bond is strongly interacting with the C_2H_2 reactant. One might expect, therefore, that the NO_2^+ bend angle should be less important. Furthermore, because reaction requires ON–O bond scission, one might expect enhancement of a strippinglike mechanism from stretching, particularly the asymmetric stretch (001) which is clearly is coupled to the reaction coordinate, and the highest energy mode. As shown in Fig. 4, however, the whole pattern of mode effects is qualitatively similar over the entire range of E_{col} , despite the changes in available energy, reaction mechanism, and collision time. It would seem, therefore, that neither vibrationally driven distortion toward the TS1 geometry nor energy in vibrational motion can directly account for the large and mode-specific vibrational enhancements observed. The suggestion is that vibration, particularly the bend, has some other indirect mechanism for influencing the dynamics.

The fact that NO_2^+ is linear, but NO_2 is bent at 135° , suggests that NO_2^+ bending excitation might facilitate temporary intrareactant charge transfer during the collision, by lowering the energy difference between the $\text{NO}_2^+ + \text{C}_2\text{H}_2$ and $\text{NO}_2 + \text{C}_2\text{H}_2^+$ states. To the extent that charge transfer occurs during collisions, it should enhance reactivity, because it converts the system from one consisting of two closed-shell reactants ($\text{NO}_2^+ + \text{C}_2\text{H}_2$) to one with both reactants open shell ($\text{NO}_2 + \text{C}_2\text{H}_2^+$). A similar mechanism was noted in trajectory calculations on the $\text{NO}_2^+ + \text{Kr}$ system, and found to have a dramatic effect on CID consistent with experiment.² If the $\text{Kr}^+ + \text{NO}_2$ charge state is accessed during a trajectory, the strong $\text{Kr}^+ - \text{ONO}$ interaction results in temporary Kr–O bond formation, leading to efficient translational-to-vibrational energy transfer, and ultimately to dissociation. In the case of $\text{NO}_2^+ + \text{Kr}$, the $\text{NO}_2 + \text{Kr}^+$ state lies 4.41 eV above reactants (at infinite separation), such that significant interreactant charge transfer occurs only if NO_2^+ becomes strongly distorted along the bending, and to a lesser extent, symmetric stretching coordinates during collision. This requirement for distortion leads to a substantial enhancement from both bending and symmetric stretching excitations, in both experiment and trajectory calculations.² [The (001) state was not studied in that system.]

In the present system, O-abstraction in the $\text{C}_2\text{H}_2^+ + \text{NO}_2$ charge state, with or without subsequent charge transfer between the products, could efficiently generate both sets of observed products. Note, however, that the $\text{NO}_2 + \text{C}_2\text{H}_2^+$ charge state lies only 1.8 eV above reactants at infinite separation. Therefore, we might expect that substantial charge transfer (i.e., delocalization) should occur in most collisions,

regardless of whether the NO_2^+ distorts strongly or not. Indeed, in complexes such as RC, the charge is distributed $\sim 65:35$ between the NO_2 and C_2H_2 moieties, reflected in the fact that the NO_2 bend angle (155°) is intermediate between that in NO_2^+ (linear) and NO_2 . It is unclear, therefore, whether a vibrationally induced charge transfer mechanism might still explain the strong effects of vibration in this system. In addition, such a mechanism does not obviously explain why the (02^20) state is so much less reactive than the (02^00) state, or why the symmetric stretch has so little effect, compared to the effect it has on CID in Kr collisions. A detailed trajectory study, investigating the origin of the strong high E_{col} mode effects, is underway.

Of particular interest is the factor of ~ 2 suppressing effect of the angular momentum associated with the (02^20) state. As noted in the Introduction, there have been only two studies of the effects of bending angular momentum on reactions,^{2,5} and the effects were small-to-negligible, as might be expected from the fact that both the angular momentum and associated energy differences were trivial compared to the angular momentum and energy of collisions. The origin of the large difference in reactivity between the (02^00) and (02^20) states is not obvious, but it is useful to consider the nature of the classical vibrational motion. To give a somewhat more realistic (but still classical) picture of the motion, we calculated trajectories of the NO_2^+ vibrational motion in different quasiclassical initial states, using force constants evaluated at the PBE1PBE/6-311G** level of theory. The analysis of collision trajectories will be presented in a future publication. The NO_2^+ zero-point motion explores ONO angles between 160° and -160° , however, the reactant is most probably found in near-linear geometry around 175° . In the (02^00) state, the angular range explored increases to $\pm 148^\circ$, with the reactant most probably found in the rather broad range between 155° and 165° . Classically, the (02^20) state rotates at the vibrational frequency at fix bend angle, however, when zero-point motion is included, the quasiclassical motion explores an angular range between 150° and 170° , with most probable angle around 160° and no probability for being linear.

What is different about the (02^20) state, therefore, is that the NO_2^+ never bends to small ONO angles, and that its plane is rotating rapidly ($\tau_{\text{bend}} \sim 54$ fs). Either factor could potentially reduce reactivity. For example, if distorting to a small ONO angle is important in driving reaction (perhaps by charge transfer), then the considerably smaller ONO angle reached in the (02^00) state would tend to make it more reactive. Note that the ONO angle in the (02^20) state is similar to the minimum ONO angle reached in the (010) state. If the ONO angle at some critical time in the collision is the critical factor, then we might expect that the (02^20) state should be somewhat more reactive than the (010) state, because it spends all its time at the minimum ONO angle, whereas the (010) state reaches its minimum angle for only a fraction of each vibrational period. This expectation is correct, as shown in Fig. 4. A “maximum distortion” mechanism seems plausible at low E_{col} . At high E_{col} , however, where the vibrationally driven distortions are presumably small compared to those driven by the collision dynamics, and where

the system reacts with reasonably high efficiency even for the ground state, it is not obvious why the (02^20) state continues to be substantially less reactive than the (02^00) state.

The other possibility is that the enhancement from bending is partially canceled by the rapid rotation of the NO_2^+ . As shown in Fig. 6, the energy of the rate-limiting TS1 is greatly increased if ONO is not oriented such that the two O atoms bend toward the C_2H_2 reactant. One might, therefore, imagine that the rapid rotation of the ONO bend plane in the (02^20) state makes it difficult for the system to find the minimum energy path. Such an argument seems reasonable at low energies, where the collision time is long compared to τ_{bend} . In particular it seems likely that in a complex such as RC, where the reactant approach is one of the low frequency modes of the complex, that rotation of ONO on a faster time scale would make finding TS1 unlikely. At high E_{col} , where the collision time becomes short and the reactivity less dependent on orientation (reaction efficiency $>25\%$), it is harder to see why ONO rotation should continue to have a large suppressing effect.

ACKNOWLEDGMENTS

This work was supported by the National Science Foundation (CHE-0110318 and CHE-0647124).

- ¹R. J. Green, H.-T. Kim, J. Qian, and S. L. Anderson, *J. Chem. Phys.* **113**, 4158 (2000).
- ²J. Liu, B. W. Uselman, J. M. Boyle, and S. L. Anderson, *J. Chem. Phys.* **125**, 133115 (2006).
- ³J. Liu, B. Van Devenner, and S. L. Anderson, *J. Chem. Phys.* **123**, 204313/1 (2005); J. Liu, K. Song, W. L. Hase, and S. L. Anderson, *J. Phys. Chem. A* **109**, 11376 (2005); J. Liu, B. Van Devenner, and S. L. Anderson, *J. Chem. Phys.* **121**, 11746 (2004); J. Liu, B. Uselman, B. Van Devenner, and S. L. Anderson, *J. Phys. Chem. A* **108**, 9945 (2004); J. Liu, K. Song, W. L. Hase, and S. L. Anderson, *J. Am. Chem. Soc.* **126**, 8602 (2004); J. Liu and S. L. Anderson, *J. Chem. Phys.* **120**, 8528 (2004); J. Liu, K. Song, W. L. Hase, and S. L. Anderson, *J. Chem. Phys.* **119**, 3040 (2003).
- ⁴B. J. Orr, *Chem. Phys.* **190**, 261 (1995); A. E. Depristo and L. C. Geiger, *Surf. Sci.* **176**, 425 (1986); D. C. Clary, *J. Chem. Phys.* **75**, 209 (1981).
- ⁵C. Kreher, R. Theinl, and K.-H. Gericke, *J. Chem. Phys.* **104**, 4481 (1996).
- ⁶B. Uselman, J. Liu, J. Boyle, and S. Anderson, *J. Phys. Chem.* **110**, 1278 (2006).
- ⁷Y.-H. Chiu, H. Fu, J.-T. Huang, and S. L. Anderson, *J. Chem. Phys.* **102**, 1199 (1995).
- ⁸J. Liu, H.-T. Kim, and S. L. Anderson, *J. Chem. Phys.* **114**, 9797 (2001).
- ⁹M. J. Frisch, G. W. Trucks, H. B. Schlegel, G. E. Scuseria, M. A. Robb, J. R. Cheeseman, J. J. A. Montgomery, T. Vreven, K. N. Kudin, J. C. Burant, J. M. Millam, S. S. Iyengar, J. Tomasi, V. Barone, B. Mennucci, M. Cossi, G. Scalmani, N. Rega, G. A. Petersson, H. Nakatsuji, M. Hada, M. Ehara, K. Toyota, R. Fukuda, J. Hasegawa, M. Ishida, T. Nakajima, Y. Honda, O. Kitao, H. Nakai, M. Klene, X. Li, J. E. Knox, H. P. Hratchian, J. B. Cross, C. Adamo, J. Jaramillo, R. Gomperts, R. E. Stratmann, O. Yazyev, A. J. Austin, R. Cammi, C. Pomelli, J. W. Ochterski, P. Y. Ayala, K. Morokuma, G. A. Voth, P. Salvador, J. J. Dannenberg, V. G. Zakrzewski, S. Dapprich, A. D. Daniels, M. C. Strain, O. Farkas, D. K. Mallick, A. D. Rabuck, K. Raghavachari, J. B. Foresman, J. V. Ortiz, Q. Cui, A. G. Baboul, S. Clifford, J. Cioslowski, B. B. Stefanov, G. Liu, A. Liashenko, P. Piskorz, I. Komaromi, R. L. Martin, D. J. Fox, T. Keith, M. A. Al-Laham, C. Y. Peng, A. Nanayakkara, M. Challacombe, P. M. W. Gill, B. Johnson, W. Chen, M. W. Wong, C. Gonzalez, and J. A. Pople, *GAUSSIAN 03* (Gaussian, Inc., Pittsburgh PA, 2003).
- ¹⁰L. Zhu and W. L. Hase, QCPE 644, a general RRKM program (Chemistry Department, University of Indiana, Bloomington, 1993).
- ¹¹S. G. Lias, in *NIST Standard Reference Database Number 69*, edited by P. J. Linstrom and W. G. Mallard (National Institute of Standards and Tech-

- nology, Gaithersburg, MD, 2003); <http://webbook.nist.gov>.
- ¹²A. Ding, A. Henglein, and K. Lacmann, *Z. Naturforsch. A* **23**, 779 (1968).
- ¹³G. A. Fisk, J. D. McDonald, and D. R. Herschbach, *Discuss. Faraday Soc.* **44**, 228 (1967).
- ¹⁴F. Bernardi, F. Cacace, G. de Petris, F. Pepi, I. Rossi, and A. Troiani, *Chem.-Eur. J.* **6**, 537 (2000).
- ¹⁵L. Zhu and W. L. Hase, *Quant. Chem. Prog. Exchange*, QCPE 644, a general RRKM program (Quantum Chemistry Program Exchange, Bloomington, IN, 1993).
- ¹⁶K. P. Huber and G. Herzberg, *Molecular Spectra and Molecular Structure IV. Constants of Diatomic Molecules* (Van Nostrand Reinhold, New York, 1979).
- ¹⁷E. R. Grant, *J. Mol. Spectrosc.* **175**, 203 (1996).
- ¹⁸S. L. Anderson, *J. Chem. Phys.* **112**, 5717 (2000).
- ¹⁹S. G. Lias, J. E. Bartmess, J. F. Liebman, J. L. Holmes, R. D. Levin, and W. G. Mallard, in *NIST Chemistry WebBook, NIST Standard Reference Database Number 69*, edited by W. G. Mallard and P. J. Linstrom (National Institute of Standards and Technology, Gaithersburg, MD, 2000); <http://webbook.nist.gov>.